J. Mol. Biol. (1996) **263**, 607–623

JMB

The Structure of an Open State of β-Actin at 2.65 Å Resolution

John K. Chik[1], Uno Lindberg[2] and Clarence E. Schutt[1]*

[1]*Henry H. Hoyt Laboratory Department of Chemistry Princeton University Princeton, NJ 08544, USA*

[2]*Department of Zoological Cell Biology, WGI Arrhenius Laboratories for Natural Sciences, Stockholm University, S-10691 Stockholm, Sweden*

**Corresponding author*

The structure of an ''open state'' of crystalline profilin:β-actin has been solved to 2.65 Å by X-ray crystallography. The open-state crystals, in 1.8 M potassium phosphate, have an expanded unit cell dimension in the *c* direction of 185.7 Å compared with 171.9 Å in the previously solved ammonium sulphate-stabilized ''tight-state'' structure. The unit cell change between the open and the tight states is accompanied by large subdomain movements in actin. Furthermore, the nucleotide in the open state is significantly more exposed to solvent, and local conformational changes in the hydrophobic pocket surrounding cysteine 374 occur during the transition to the tight state. Significant changes were observed at the N terminus and in the DNase-I binding loop. Neither the structure of profilin nor its contact with β-actin are affected by the changes in the unit cell. Applying osmotic pressure to profilin:β-actin crystals brings about a collapse of the unit cell comparable with that seen in the open to tight-state transition, enabling an estimate of the work required to cause this transformation of β-actin in the crystals. The slight difference in energy between the open and collapsed states explains the extreme sensitivity of profilin:β-actin crystals to changes in chemical and thermal environment.

Keywords: β-actin; profilin; actin filaments; conformational changes; domain motions

Introduction

The motile behaviour of eukaryotic cells is highly dependent on the dynamic properties of the actin-based microfilament system. The assembly of actin into helical filaments is accompanied by conformational changes and hydrolysis of its bound ATP (Oosawa, 1983; Korn *et al*., 1987). The exchange of the actin-bound nucleotide *in vitro* is accelerated by profilin, a protein of molecular mass 12 to 15 kDa (Carlsson *et al*., 1977; Reichstein & Korn, 1979; Mockrin & Korn, 1980; Goldschmidt-Clermont *et al*., 1992; Machesky & Pollard, 1993). In the physiological functioning of the microfilament system, the polymerizability of actin is influenced by profilin, and other factors such as thymosin β4 (Safer *et al*., 1991, Cassimeris *et al*., 1992). Profilin interacts with phosphoinositides, important lipid intermediates in the generation of ''second'' messengers (Berridge, 1993), which *in vitro* destabilize the profilin:actin heterodimer (Lassing & Lindberg, 1985, 1988). This interaction appears to be part of a dual control mechanism, regulating both actin polymerization and the hydrolysis of phosphoinositides through the inhibitory effect of profilin on phospholipase Cγ1 (Goldschmidt-Clermont *et al*., 1990, 1991, 1992). Profilin:actin heterodimers preferentially bind to the barbed, fast-growing ends of actin filaments (Pring *et al*., 1992; Pantaloni & Carlier, 1993), whose accessibility appears to be controlled *in vivo* by receptor-mediated transmembrane signalling pathways (Hartwig *et al*., 1995; Tardif *et al*., 1995).

Profilin in complex with either β or γ-actin can be isolated from non-muscle cells and crystallized (Carlsson *et al*., 1976; Segura & Lindberg, 1984; Lindberg *et al*., 1988). The profilin:β-actin crystal unit cell is extremely sensitive to variations in the ionic strength and pH of the crystal bathing solution, in the temperature, and in the type of nucleotide used in crystallization (Schutt *et al*., 1989). Although large and well diffracting crystals were obtained in potassium phosphate buffers in the presence of ATP and divalent cations, it was

Present address: J. K. Chik, The National Institutes of Health, DCRT/LSB, Bldg. 12A Rm. 2041, 12 South Dr. MSC 5626, Bethesda, MD 20892-5626, USA.

0022–2836/96/440607–17 $25.00/0

difficult to find conditions for stabilizing the unit cell of the crystals. However, transfer of the crystals into high ionic strength ammonium sulphate solutions (tight state) resulted in crystals stable enough for isomorphous heavy-atom derivatization (Schutt *et al*., 1989). The crystal structure of the bovine profilin:β-actin complex in the tight state was solved to 2.55 Å resolution (Schutt *et al*., 1993).

The remarkable fact that these crystals diffract to high resolution over a broad range of unit cell dimensions can be rationalized in terms of a cooperative network of actin molecules in the crystals (Schutt *et al*., 1989). The variability of the crystalline unit cell dimensions appears to be solely due to inherent properties of actin itself, since the crystal structure of profilin in the unbound state is nearly identical with that in the profilin:β-actin crystals (Cedergren-Zeppezauer *et al*., 1994). Although profilin:β-actin is heterodimeric in solution, actin monomers make extensive contacts with one another about the 2_1 axis along the *b* direction in profilin:β-actin crystals. The ATP-bound β-actin ''ribbons'' are thought to represent a metastable state that can be transformed into classical ADP-containing helical filaments by conformational changes within actin monomers (Schutt *et al*., 1989, 1995a). This structural model accounts for the profilin-catalysed assembly at the barbed end of actin filaments (Cedergren-Zeppezauer *et al*., 1994) seen *in vitro* (Pring *et al*., 1992; Pantaloni & Carlier, 1993) and in permeabilized cells (Tardif *et al*., 1995).

Actin is part of a family of proteins with similar folding topology that includes hexokinase, Hsc70 and glycerol kinase (Flaherty *et al*., 1991; Kabsch & Holmes, 1995). By analogy with hexokinase (Bennett & Steitz, 1980), actin is expected to have open and closed states. Comparison of tight-state β-actin extracted from the profilin:β-actin crystal structure (Schutt *et al*., 1993) with α-actin from the DNase I:α-actin structure (Kabsch *et al*., 1990) revealed a 5° relative rotation of the two major domains of actin. However, there was no significant conformational difference in the nucleotide-binding cleft, indicating that actin in the two complexes is in the same state of closure relative to the bound nucleotide. The availability of the high-resolution structure of bovine profilin:β-actin in the tight state (Schutt *et al*., 1993) makes possible structure determinations *via* molecular replacement (Rossmann & Blow, 1958) of the various states of the profilin:β-actin that can be prepared by transferring crystals to solutions of different composition (Schutt *et al*., 1989). We report the structure of an open state of β-actin, defined by the greater solvent accessibility of the nucleotide phosphate groups, in which there are significant conformational differences compared with the previously determined tight-state structure. Comparison of these crystallographically distinct states shows that actin can adopt different conformations by hinged subdomain movements. Structural changes distributed throughout the actin molecule are directly linked to changes in the binding of nucleotide phosphate groups in the central cleft.

Results

Unit cell variation of profilin:β-actin crystals

The volume of the unit cell of profilin:β-actin crystals is extremely sensitive to the ionic composition of the medium in which the crystals are bathed. Changes in the unit cell were observed with profilin:β-actin crystals in $(NH_4)_2SO_4$ upon lowering the pH (Carlsson, 1979) or by increasing the ionic strength (Schutt *et al*., 1989). As shown by Carlsson (1979), addition of 0.5 M potassium phosphate abolishes the effect of pH on the unit cell of crystals grown in 1.3 M $(NH_4)_2SO_4$. This was found also for crystals grown in potassium phosphate buffer. For ten different crystals spanning the pH range 6.03 to 7.49, the unit cell dimensions remained around 38.15 ($\pm$0.8) Å $\times$ 72.27 ($\pm$0.2) Å $\times$ 184.9 ($\pm$0.8) Å.

The dependence of cell volume on ionic conditions was also re-examined. Figure 1(a) shows how the cell dimensions (expressed as percentages) depend on the concentration of potassium phosphate. The most striking change is seen in the value of the *c*-dimension, which decreases by 6% as the molarity is changed from 1.8 M to 3.6 M KPO_4, pH 7.3 (unit cell change in the *c*-direction of 185.7 Å to 173.4 Å). A partial structure of the 3.6 M KPO_4 state has been solved (Chik, 1996). Evidence for a specific ammonium ion effect on the unit cell is given in Table 1.

Osmotic stress could contract the unit cell of the crystals to a degree similar to that induced by specific chemical perturbations. Figure 1(b) shows that a sharp transition in the volume of the unit cell occurs between 0.0300 g and 0.0375 g of dextran/ml. The change in unit cell volume is 2.2×10^4 Å^3 (4.3%; unit cell change in the *c*-dimension is 184.9 Å to 174.8 Å), roughly equivalent to the change occurring during the open to tight-state transition. Assuming that dextran is excluded from the crystals, while all other solutes and solvent are in free exchange, the osmotic pressure can be determined from standard calibration curves. Calibration curves were available only for 40 kDa and 110 kDa dextran so that interpolation was used for the 60 kDa dextran used in the present experiments. The osmotic pressures for 40 kDa (M. Prouty & R. Podgornik, personal communication) and 110 kDa (C. Bonnet-Gonnet, personal communication) dextrans, respectively, are given by:

$$\log P_{40} = 3.009 + 0.9762w^{0.393}$$

$$\log P_{110} = 1.385 + 2.185w^{0.2436}$$

where w is the weight percentage of the dextran, and P_{40} and P_{110} are the osmotic pressures in dynes/cm^2. Using these expressions, the osmotic pressure for 3.0% (w/w) 60 kDa dextran lies

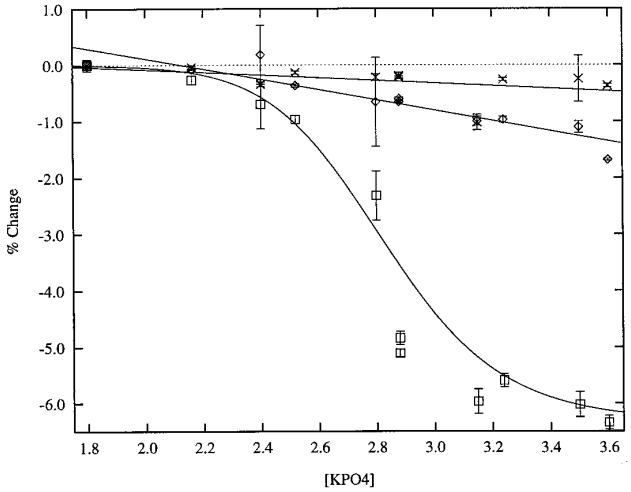

(a)

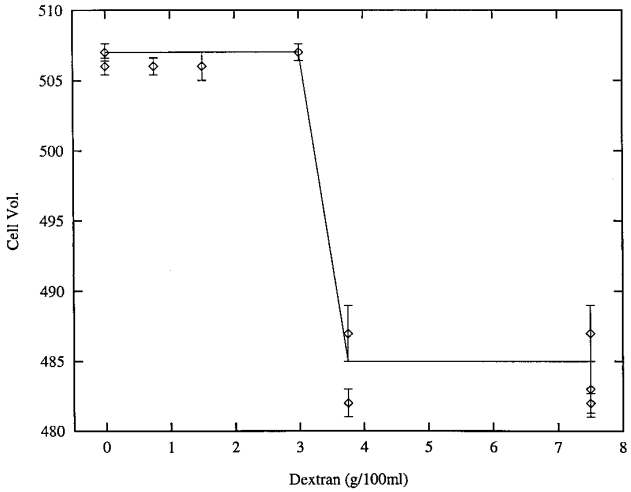

(b)

Figure 1. (a) Dependence of the unit cell dimensions of the profilin:β-actin crystals expressed as a percentage of the open-state value as a function of potassium phosphate concentration at pH 7.3. The curve going through the *c*-axis value was generated using a Hill equation fixing the mid-point at 2.83 M. The resultant Hill coefficient was 14.0. Symbols: *a*-dimension, open diamonds; *b*-dimension, ×; *c*-dimension, open squares. (b) Dependence of the unit cell volume (1000 Å^3) of the profilin:β-actin crystals as a function of the concentration of dextran. Below 3.0 g of dextran / 100 ml, the unit-cell dimensions were 38.23 (±0.03) Å × 72.24 (±0.2) Å × 185.6 (±0.6) Å. Above 3.75 g / 100 ml they were 38.63 (±0.1) Å × 71.80 (±0.2) Å × 174.8 (±0.8) Å.

between 3.3×10^5 and 1.7×10^5 dynes / cm^2. Therefore, the work required to contract the unit cell by 4.3% during the cooperative transition in the crystal is between 104 and 52 cal per mole unit cell. This is only a fraction of thermal energy at 20°C (600 cal / mol). The molecules all undergo this low-energy transformation in concert as indicated by the sharpness of the diffraction pattern to high resolution (Chik, 1996). The extreme sensitivity of profilin:β-actin crystals in phosphate buffers to

Table 1. Unit-cell dimension of profilin:β-actin crystals in open-state buffer with different salts added

State	*a*	*b*	*c*
Control[a]	38.15 (±0.01)	72.33 (±0.04)	184.5 (±0.2)
1.5 M KCl[b]	38.13 (±0.03)	72.38 (±0.03)	183.3 (±0.3)
2.0 M NaCl	38.06 (±0.02)	72.30 (±0.07)	182.1 (±0.4)
2.0 M NH_4Cl	38.85 (±0.01)	71.50 (±0.04)	174.3 (±0.3)

[a] "Control" means cell dimensions in open-state buffer without extra added salts.

[b] Control and 2.0 M NaCl unit cell values are averages of measurements on three crystals, while 1.5 M KCl and 2.0 M NH_4Cl values are from measurements on two crystals each.

"thermal bursts" (Schutt *et al*., 1989) can now be explained in these terms.

Subdomain orientations in the open and tight states

Comparison of the structures at the two end-points of the transition from the open to the tight state shows how conformational changes in the actin molecule can accommodate the unit cell changes in the crystal. Figure 2 shows the C$^\alpha$ backbone trace of the open-state profilin:β-actin structure. Table 2 shows the rms difference between the C$^\alpha$ coordinates of the large and small domains and the four subdomains of actin for the two states as calculated in LSQKAB (Collaborative Computational Project, 1994; Kabsch, 1976). This indicates that, for the most part, the secondary structure is little changed during the open to tight-state transition. Table 2 shows that the rms difference in C$^\alpha$ coordinates for profilin in the two states is only 0.54 Å, which is comparable with the difference between free and actin-bound profilin when the N-terminal "switch" of profilin (Cedergren-Zeppezauer *et al*., 1994, Schutt *et al*., 1995a) is excluded from the calculation. The primary profilin:β-actin interface shows little change after transition from the open state to the tight state as judged by the excellent agreement in the positions of profilin residue His119, and the surrounding β-actin side-chains of Y169, M355 and F375 (Figure 3). Aromatic amino acid side-chains in the vicinity of C374 show relatively small movements, except for W356, which becomes completely buried in the tight state.

The constancy of the profilin structure provides a convenient reference for considering the relative motions of the domains and subdomains between the two states of β-actin. Figure 4(a) shows actin after of aligning the C$^\alpha$ coordinates of profilin from the tight-state complex with those of the open state. Using the profilin-aligned β-actin structures, the directional cosines of the rotations necessary to superimpose the domains and subdomains individually are presented in Table 3 and in Figure 4(b). The transition between the open and tight states involves a relative rotation of the two domains of actin of approximately 9.6° about an axis roughly parallel with the *a*-axis, i.e. a

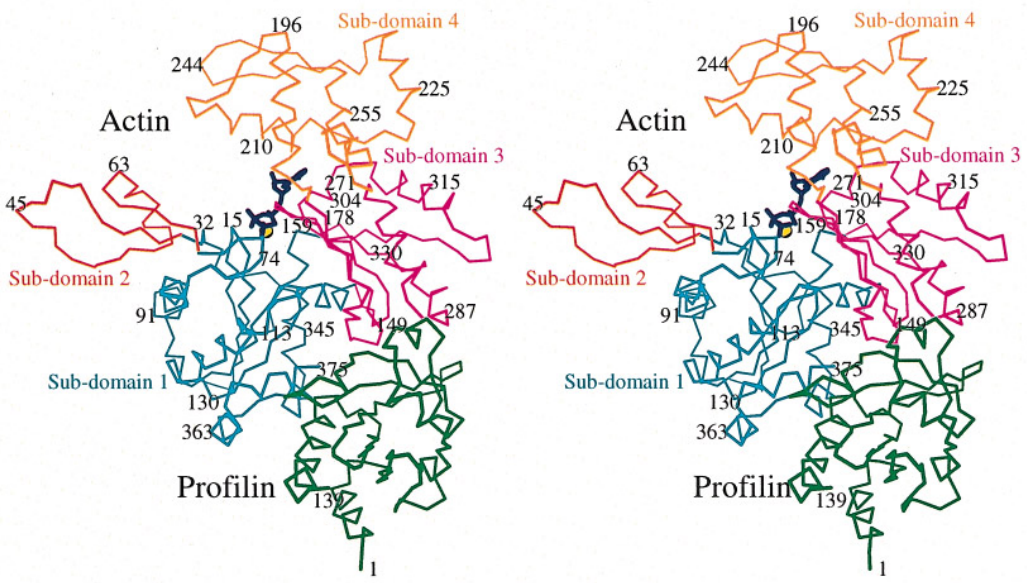

Figure 2. A stereo view of the C^{α} trace of the open state of profilin:β-actin with ATP and Ca^{2+}. The complex is oriented with the crystal *b*-axis vertical and the *c*-axis horizontal. Actin residues are numbered according to the α-actin convention (i.e. N-terminal residue is D2). Profilin (green) is numbered 1 to 139. The subdomains of actin as defined in the Figure are: 1 (cyan) residues 2 to 34, 70 to 145 and 334 to 375; 2 (red) 34 to 70; 3 (purple) 145 to 179, 272 to 334; 4 (orange) 179 to 272. All molecular representations were made in MOLSCRIPT (Kraulis, 1991).

cleft-closure by 9.6°. As seen from Table 3, the closure of the cleft is principally due to a 14.7° rotation of subdomain 2. The subdomains execute independent motions during the transition from the open to the tight state, i.e. the two domains do not move as integrated units. Subdomain 2 rotates by 14.7° about the *a*-axis, while subdomain 1 rotates only by 2.8° about an axis pointing in a direction 67° away. There is a 28° difference in the direction of the axes about which subdomains 3 and 4 rotate.

The ribbon organization of β-actin is preserved during the open to tight-state transition, despite the fact that subdomain 2, which participates in the ribbon contact, undergoes a 14.7° rotation. The only significant intermolecular contacts along the *a*-direction occur between profilin molecules organized into 2_1 columns. Owing to the tight binding between profilin and β-actin ribbons, the effect of these profilin:profilin contacts is to integrate a highly cooperative three-dimensional meshwork of proteins. The buckling and rotation of the ribbon during the open to tight-state transition is accompanied by a slight rotation of the profilin columns. The only contacts between ribbons in the *a*-direction are ''grazing'' interactions involving side-chains from subdomain 2 and the N terminus. The open to tight-state transition involves a contraction of the crystal unit cell of 13.8 Å along the *c*-axis as the ribbon axes move closer together. Viewing the crystal structures down the *b*-axis (Figure 5) shows that the changes in the *c*-dimension are mainly due to a global rotation of 6° about the 2_1 axis parallel with the *b*-direction.

Table 2. C^{α} comparison of various structural elements of open and tight-state profilin:β-actin

Region	rms (Å)
Profilin:β-actin (w/o DNase loop 39–53 and 1–8)	1.41
Large domain (150–331)	0.90
Small domain (8–32, 52–144 and 338–375)	0.83
Profilin	0.55
Sub-domain 1 (8–32, 79–144 and 338–375)	0.45
Sub-domain 2 (35–38 and 52–69)	0.72
Sub-domain 3 (150–178 and 273–331)	0.56
Sub-domain 4 (181–262)	1.13

Differences in local conformation

Other differences in local conformation of profilin:β-actin between the open and the tight state generally occur in loop regions and regions with high *B*-factors (Figures 6 and 12). The N terminus, residues 2 to 7, is quite different between the two states, adopting a helical structure in the tight state and a turn in the open state. The reason for this is that the N-terminal residues in the open state are in closer contact with subdomain 2 on monomer N – 1 than in the tight state. The DNase I-binding loop, residues 39 to 51, is very different in the two states (see Figure 7). The electron density map in this region was difficult to interpret, and the main-chain *B*-factors were high. Residues found at the top of subdomain 4 also have high *B*-factors in the open-state β-actin and all other actin structures solved to date (Kabsch *et al*., 1990; McLaughlin, 1993; Schutt *et al*., 1993). In particular, residues 196 to 206 and 231 to 235 are in different conformations

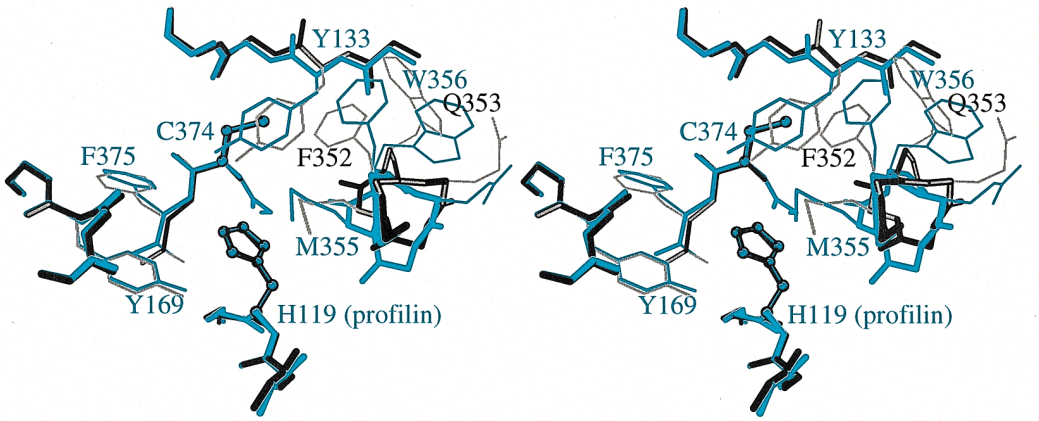

Figure 3. Stereo view of β-actin amino acid residues surrounding histidine 119 of profilin in the open and tight states of the profilin:β-actin crystal. Colour scheme: the open (cyan) and tight (black) states. The molecules were aligned by superimposing the C^{α} atoms of profilin of the two states (main chain, thick lines; selected side-chain atoms, thin lines). The side-chains of H119 and C374 are depicted using ball-and-stick representations. Hydrogen atoms are not drawn.

in the two states of profilin:β-actin. In addition, the turn in the β-hairpin, residues 242 to 245, is more closed in the tight state. In the tight state, the carbonyl group of L242 is 3.0 Å from the main-chain amide group of G245, whereas in the open state this distance is 4.5 Å, indicating that a hydrogen bond is missing in the open state. The loop consisting of residues 322 to 325 is in an altered conformation (not shown).

The two major domains in the actin fold are connected by two short polypeptides, residues numbered 145 to 150 and 332 to 337 (Figure 2). The 145–150 region of the sequence is nearly identical in both open and tight states of the crystal. The 332–337 region, on the other hand, undergoes a progressive lengthening as judged by the distance between the C^{α} atoms of P331 and S338. In the DNase I:α-actin structure this distance is 10.0 Å. It expands slightly in tight state β-actin to 10.2 Å, and is 10.5 Å in the open state, as shown in Figure 8. Residues 332 to 337 can be classified as an (I, I + 2) double β-turn (Hutchinson & Thornton, 1994), in which E334 and R335 constitute residues i + 2 and i + 3 of the first turn and i' and i' + 1 of the second turn. The phi / psi angles of both turns indicate that, individually, they would be classified as type I (Hutchinson & Thornton, 1994). The contraction of this segment, as seen in the open to tight-state transition, suggests that this class of secondary structure elements (''expansion joints'') may be used to relieve interdomain stresses during large-scale conformational changes.

Salt-bridge switching during the open to tight-state transition

During the transition from the open to the tight state, subdomain 2 of actin monomer N in the β-actin ribbon (Figure 9) swings away from a position where it interacts with the top of subdomain 4 of actin monomer N – 1 (across the ribbon axis) to a position where it apparently is more tightly bound to the bottom of subdomain 1 of actin monomer N + 1. In the open state, there is a ternary salt-bridge between D51 and K84 of monomer N (Figure 9) and D244 on monomer N – 1 in the actin ribbon. These salt-bridges act as ''latches'' holding subdomain 2 in position in the open state. They are not seen in the tight state, presumably because of enhanced electrostatic screening at the higher ionic strength or differences in the chaotropic properties of these Hofmeister-series salts. The breakage of these salt-bridges during the transition from the open to the tight state has two consequences: firstly, it enables subdomain 2 to move away from its own subdomain 1, and pivot about the middle strand (residues 35 to 38) of its three-stranded β-sheet; secondly, by breaking contact with subdomain 4 of monomer N – 1, subdomains 3 and 4 of monomer N – 1 can rotate about the primary hinge between the two actin domains. In the tight state there is a hydrogen bond between MeH73 and G158, which is not present in the open state owing to the greater separation between the two domains. Furthermore, in the tight state, there is an intermolecular hydrogen bond between the side-chain of H87 and the carbonyl group of P243 (Figure 9).

The salt-bridge between E257 and R312 in the tight-state structure (Schutt *et al*., 1993) appears to be even stronger in the open state of β-actin, since the distance between C^{δ} of E257 and CZ of R312 is 3.8 Å as opposed to 4.6 Å in the tight state. This salt-bridge did not appear in the original DNase I:α-actin model (Kabsch *et al*., 1990), but is present in α-actin complexed with gelsolin subfragment 1 (P. J. McLaughlin, personal communication) and in the molecular dynamics refinement of α-actin (Tirion *et al*., 1995). The maintenance of this salt-bridge during the large conformational changes in the open to tight-state transformation adds weight to the arguments (Schutt *et al*., 1995b) against

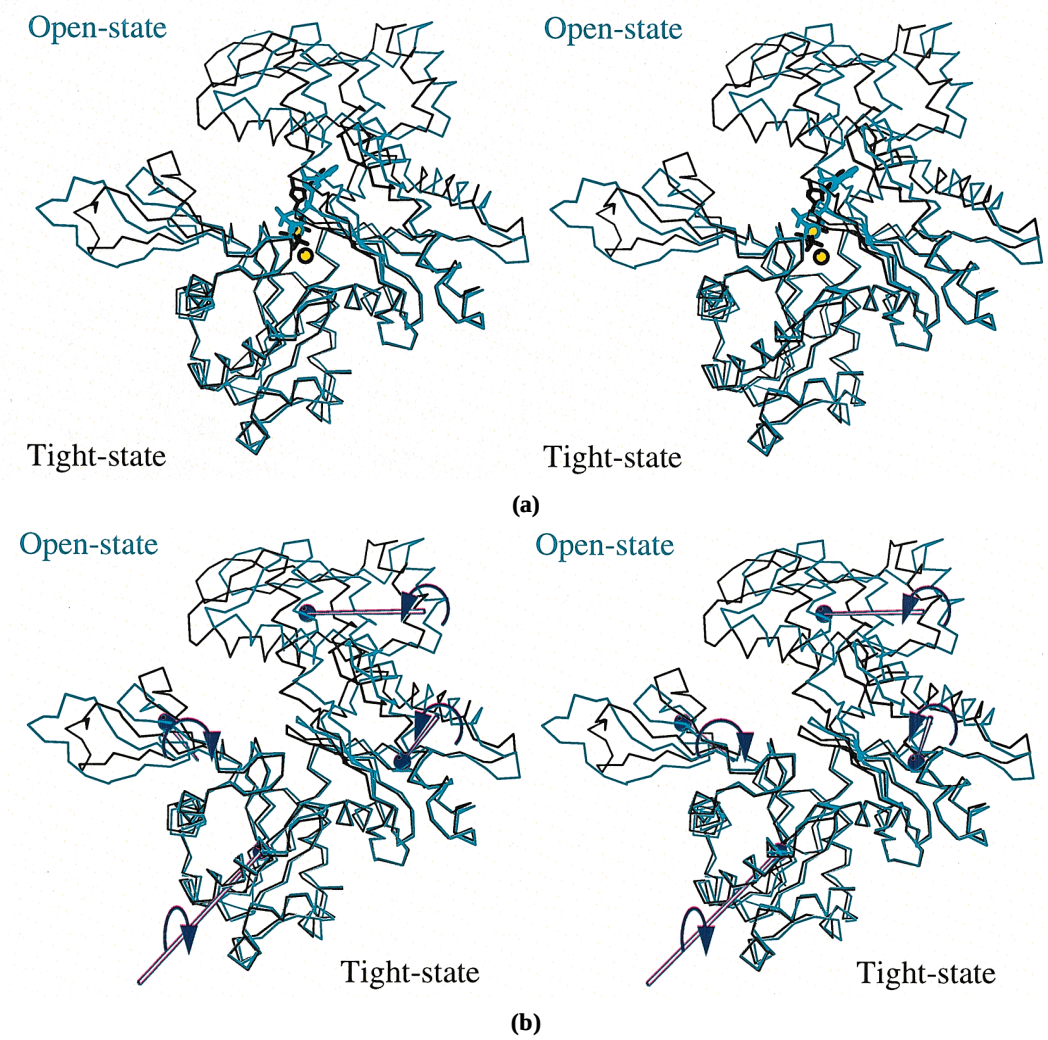

Figure 4. Stereo view comparing the C^{α} traces of the open and tight state β-actin. The actin molecules were aligned by superposition of their bound profilin (not shown). Colours: β-actin open state, cyan lines; tight state, black lines; ATP and divalent cation of the open and tight state in cyan and black, respectively. (a) The superpositioning with the adenosine moiety pointing away from the view. The calculated axes about which the subdomains of open-state β-actin rotate to superimpose onto the corresponding tight state subdomain are shown in (b) and see Table 3. The senses of the rotations about the centroids, marked by blue balls, are indicated by the arrows. The orientation of the molecules is as in Figure 2 (crystal *b*-axis vertical). Note that the rotation axis for the subdomain 2 superimposition is nearly parallel with the *a*-axis of the crystal (normal to page).

Table 3. Rotational angles and directional cosines of axes relating structural elements during the open to tight-state transition of the profilin:β-actin crystals

	Rotation			
Region	Angle (deg.)	Directional cosines of axis[a]		
Actin (minus 39–53 and 2–8)[b,c]	3.1	0.77	–0.51	0.38
Subdomains 3 + 4 (150–331)[d]	5.7	0.94	–0.10	0.32
Subdomains 1 + 2 (8–32, 52–144, 338–375)	3.9	–0.80	–0.41	0.43
Subdomain 1 (8–32, 79–144, 338–375)	2.8	–0.41	–0.66	0.63
Subdomain 2 (35–38, 52–69)	14.7	–0.96	0.19	0.20
Subdomain 3 (150–178, 273–331)	4.8	0.97	–0.23	0.12
Subdomain 4 (181–262)	5.9	0.84	–0.01	0.54

[a] The directional cosines of the rotational axes are reported with reference to the crystal unit cell axes after superimposition of profilin in the two states. Each axis passes through the centroid of the respective subdomains after alignment with LSQKAB.
[b] Actin minus the DNase I-binding loop and minus residues 2 to 8.
[c] rms 1.13 Å.
[d] Residue numbers within parentheses.

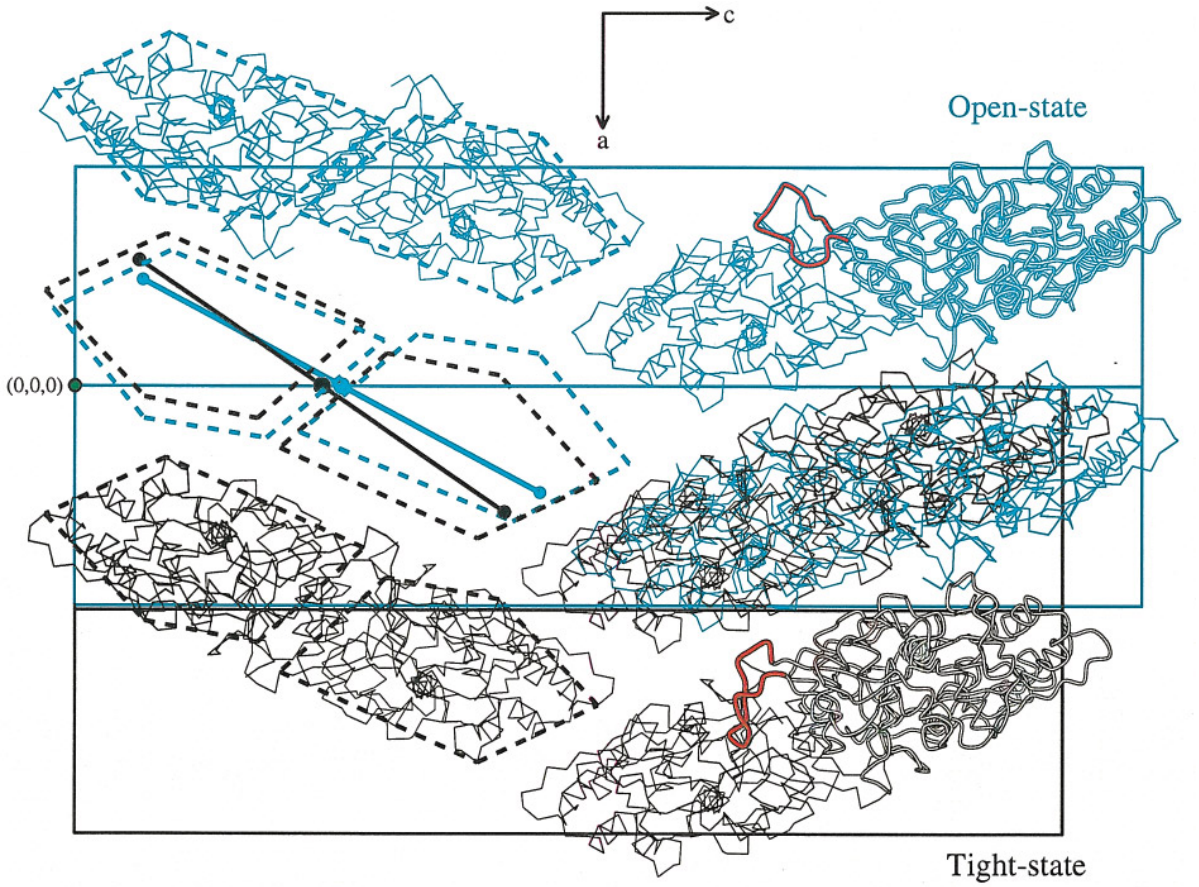

Figure 5. The C^{α} trace of β-actin projected down the *b*-axis for the open and the tight states of the profilin:β-actin crystals. Two unit cells are outlined in cyan for the open state and black for the tight state. A unit cell from each of the two states of the crystals was overlayed in the centre of the Figure with reference to a common origin marked by a green dot on the extreme left. The contraction of the unit cell in the *c*-direction is easily seen. The dotted lines in the left-hand portion of each unit cell outline the outer regions of the β-actin molecules. The outline was obtained by connecting the C^{α} atoms of residues 28, 235, 322, 270 and 38. The middle pair in the left-hand column compares the molecular outlines of the two states. A continuous line connects the centroids, represented by filled circles, of the two profilin molecules (not shown). The relative rotation about the ribbon 2_1 screw axis (large, filled, coloured circle) between the open and tight state is 6°. In the right-hand column, a monomer from each state is highlighted using a smooth unfilled tube. The flexible DNase I loop (39 to 51) is shown in red in both states. The axes are shown at the top centre of the Figure.

remodelling residues 262 to 273 into a ''hydrophobic plug'' stabilizing F-actin (Holmes *et al*., 1990).

Conformational changes in the ATP-binding site

Figure 10 compares the structures of the open and tight states in the nucleotide phosphate-binding region. In the open state the solvent-exposed surface area of the ATP phosphate groups is 52.5 $Å^2$ compared with only 1.8 $Å^2$ in the tight state. The phosphate-binding region comprises two β-hairpin loops (N12–C17 and D154–H161) protruding into the cleft between subdomains 1 and 3. During the transition to the tight state, these two loops move closer together, burying the ATP phosphate groups. The C^{α}–C^{α} distance from D157 to G15 (residues at the tips of the loops) is 8.2 Å in the open state and 5.3 Å in the tight state, Similarly, the C^{α}–C^{α} distance between G158 and S14 is 8.2 Å in the open state and 5.6 Å for the tight state. The amide group of G15 changes phosphate oxygen bonding partners in the transition from the open to the tight state (Figure 11(a) and (b)). In the open state, O2B hydrogen bonds to the amide group of Gly15, which in the tight state interacts with O1B. This ''bond-ratcheting'' results in the open-state O1B projecting into the solvent. In the tight state, O2B is directed towards the divalent cation in the cleft. The Me^{2+} ion position in the open state (Ca^{2+}) refined with high *B*-factors (113 $Å^2$). It should be noted that, in both cases, the *B*-factors of the ATP phosphate groups are also high (>80 $Å^2$). In the open state, Ca^{2+} interacts exclusively with the oxygen atoms from the ATP phosphate groups. The distances (2.3 Å) are similar to that seen in the crystal structure of CaATP (Figure 11(a), and Cini *et al*., 1984).

However, the residues coordinating the divalent cation (D11, E137 and D154) are in a similar conformation in both open and tight states.

Discussion

There is evidence that conformational changes in actin are linked to the state of the actin-associated nucleotide (Oosawa, 1983; Korn *et al*., 1987, Schutt *et al*., 1989; Egelman & Orlova, 1995). The determination of the crystal structure of α-actin revealed the strategic positioning of ATP in a cleft between two major domains, each further divided into two subdomains (Kabsch *et al*., 1990). Profilin:β-actin crystals undergo cooperative transitions depending upon chemical and physical conditions, including the state of the nucleotide (Schutt *et al*., 1989). It was evident from the crystal structure of tight-state profilin:β-actin, when compared with the DNase I:α-actin structure (Kabsch *et al*., 1990), that the two domains of actin can rotate by 5° with respect to one another without changes in the ATP-binding site (Schutt *et al*., 1993). However, the possibility was left open that this interdomain movement was attributable merely to intrinsic differences between α and β-actin. The present study on a single isoform of actin provides direct crystallographic evidence that actin can exist in both an open and a closed state, and that the conformational changes can be much larger than the 5° hinge motion and be located at other places in the molecule.

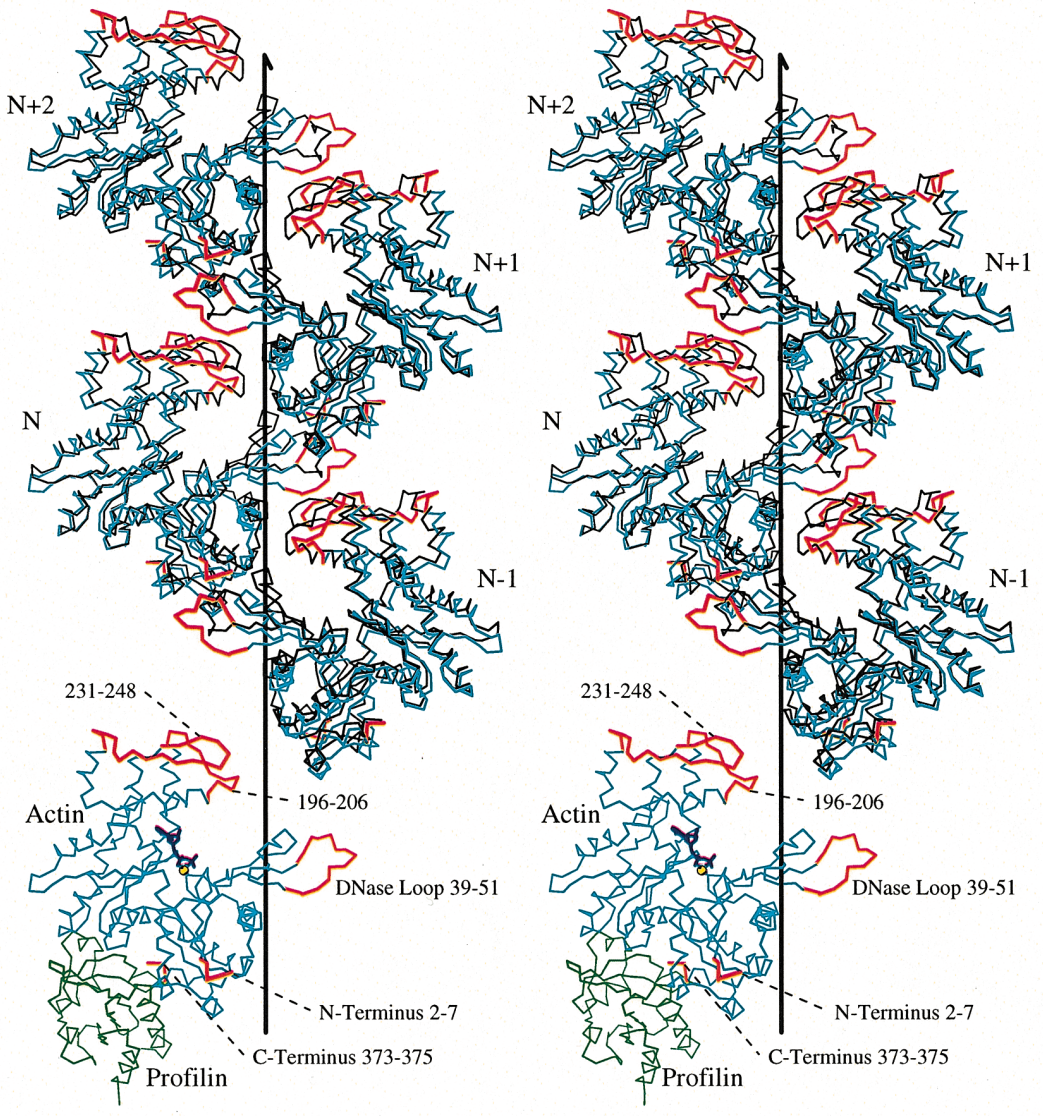

Figure 6. Stereo view of C^{α} traces of open (cyan and red) and tight (black) state β-actin ribbons. An actin tetramer from the tight state profilin:β-actin structure was aligned with that of the open state by first superimposing the ribbon 2_1 axis (thick black line). Translation along and rotation about the 2_1 was fixed by aligning profilin (not shown) centroids. The open and tight state β-actin is shown in cyan and black, respectively. Regions having high *B*-factors and/or large differences between open and tight states are highlighted in red in the open state. At the bottom of the Figure an open-state heterodimer is depicted with these regions labelled (profilin green).

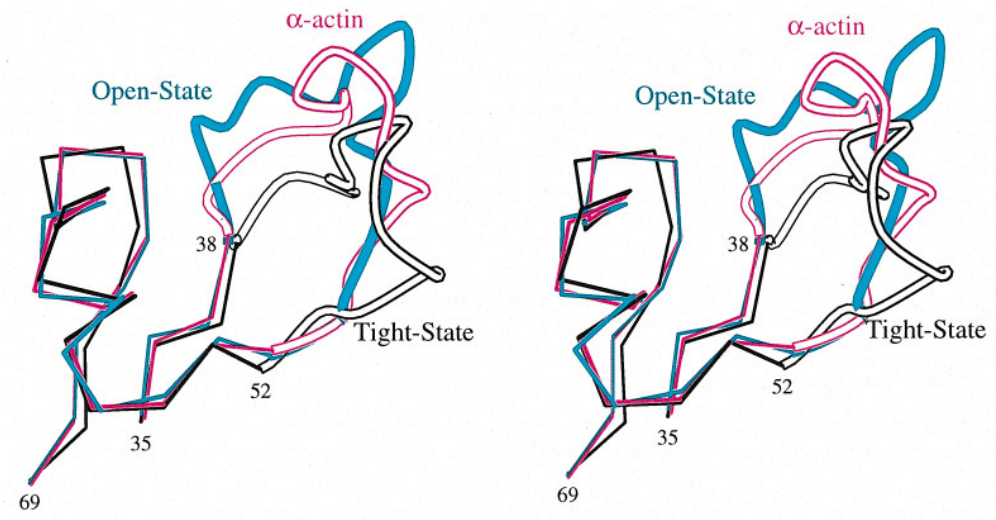

Figure 7. Stereo view of subdomains 2 of α-actin (purple), open (cyan) and tight (black) state β-actin. The DNaseI-binding loop residues 38 to 52 are represented by smooth tubes going through C^{α} positions.

The role of actin subdomain 2

The most dramatic change in the β-actin structure seen in the open to tight-state transition is the 14.7° rigid-body rotation in the orientation of subdomain 2 (Figures 4 and 7, and Table 3). The intrinsic flexibility of actin subdomain 2 is consistent with conclusions reached from a comparison of individual atomic temperature factors in three different crystalline environments (Kabsch *et al*., 1990; McLaughlin *et al*.,1993; Schutt *et al*., 1993), from detailed differences in conformation between α and β-actin (Schutt *et al*., 1993), and from molecular dynamics simulations (Tirion *et al*., 1995). This region has been implicated as being important for the generation of movement of actin filaments in *in vitro* motility assays (Schwyter *et al*., 1990).

Subdomain 2 contains the major DNase I-binding loop (Kabsch *et al*., 1990). DNase I is a potent inhibitor of actin polymerization (Lazarides & Lindberg, 1974; Hitchcock *et al*., 1976), suggesting that it can interrupt one of the actin:actin contacts in filaments (Holmes *et al*., 1990; Schutt *et al*., 1995a). Biochemical evidence indicates that this region of actin is important in forming intermonomer bonds in F-actin (Hegyi *et al*., 1974; Fievez & Carlier, 1993). The interpretation of structural changes in actin filaments, seen at low resolution by electron microscopy (Orlova & Egelman, 1992), and inferred from muscle fibre X-ray diffraction (AL-Khayat *et al*., 1995), require modifications of the Holmes' model in subdomain 2.

Changes in the nucleotide binding cleft

The tightening of the structure around the ATP phosphate groups appears to contribute to the apparent greater stability and higher order of the tight state. The DNase I:α-actin complex with either ATP or ADP bound in the α-actin cleft (Kabsch *et al*., 1990) possesses the same closed conformation about the nucleotide as seen in actin in the tight state of profilin:β-actin (Schutt *et al*., 1993). The near identity between ATP and ADP-containing α-actin in the crystallized complex with DNase I was used

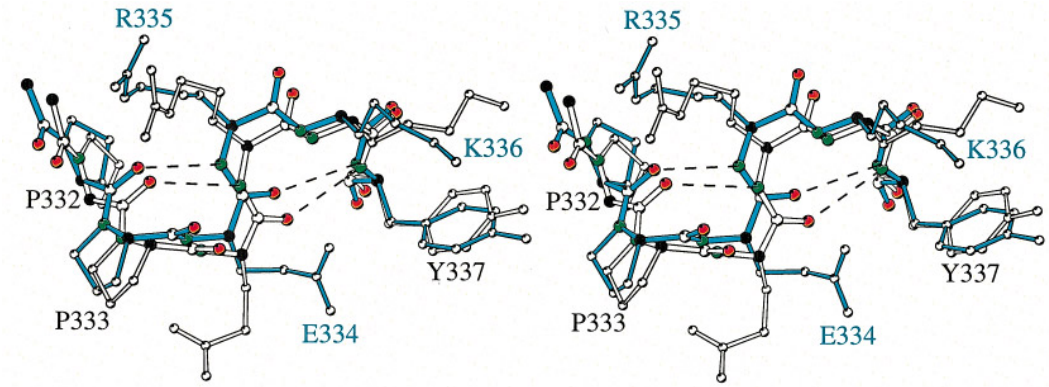

Figure 8. Stereo view of the open and tight state residues 332 to 337. Colour code: tight state (open sticks), open state (cyan sticks), C^{α} (black), main-chain carbonyl oxygen (red), main-chain nitrogen (purple), all other atoms (unfilled balls). Hydrogen atoms are not shown.

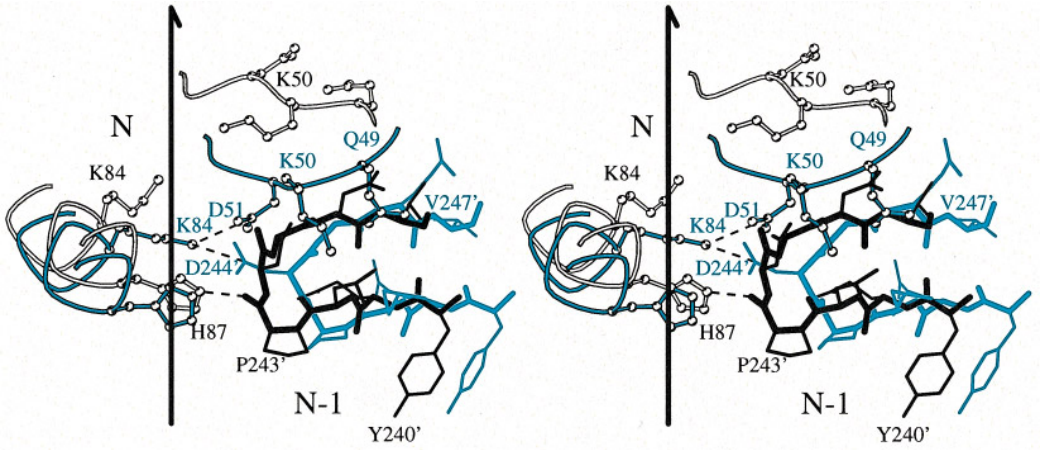

Figure 9. Stereo view of intra- and intermolecular salt-bridges around K84 in open and tight state β-actin. The open and tight states were aligned as in Figure 2. For monomer N (residues 48 to 53 and 81 to 89) the main chain of the tight state is shown as an unfilled tube with selected side-chains depicted using white balls and sticks. For the open state, cyan tubes and sticks are used. The monomer N – 1 (residues 240 to 247) are depited as thick lines with the tight state in black and the open state in cyan. The ribbon 2_1 axis is black. The direction of view is the same as in Figure 2. The N – 1 residue numbers are primed.

to justify the choice of the α-actin conformation as the starting point for modelling F-actin-ADP (Holmes *et al*., 1990). However, in the case of DNase I:α-actin, the similarity of the ATP and ADP forms arises from the ''clamping'' of the two domains at the top of the cleft by the DNase I molecule (Rozycki *et al*., 1994). In the β-actin ribbon, monomers are also bridged at the top of the cleft, but by neighbouring multidomained actin monomers that can undergo relatively large internal changes in structure *via* rotations about hinge-points without breakage of crystal contacts, enabling the cooperative changes in β-actin observed in the crystals. To date there is no high-resolution structural information concerning the unclamped ADP form of actin for any of the actin isoforms.

The actin C terminus

In the structure of tight state β-actin, the C-terminal phenylalanine residue (F375) is buried in a hydrophobic pocket, and the penultimate cysteine residue is not exposed to solvent (Schutt *et al*., 1993). However, the availability of the penultimate C374 to labelling with pyrene-iodoacetamide and 5-[2-(iodoacetamido)ethylamino]-1-naphthalene-sulfonic acid (1,5-I-AEDANS), and the

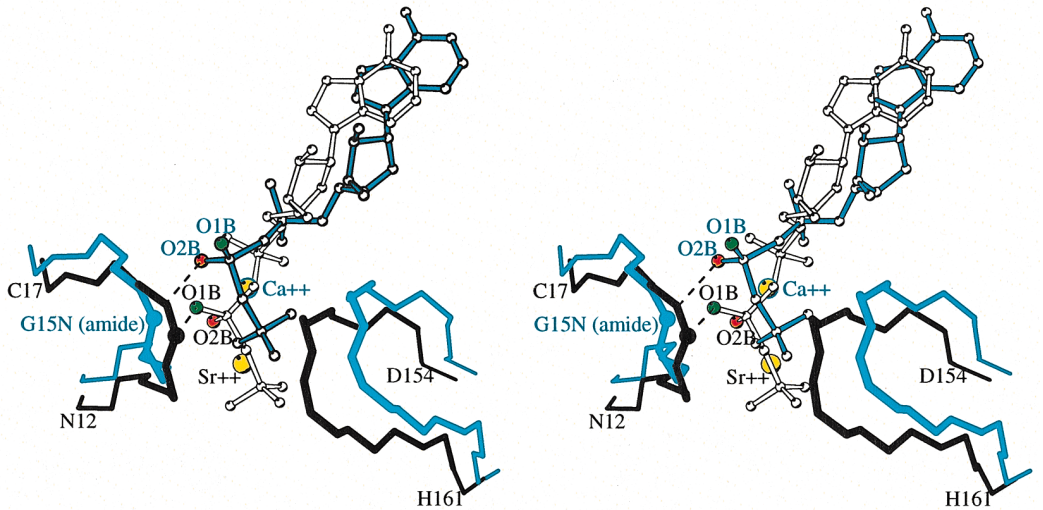

Figure 10. Stereoview of the ATP phosphate-binding site in the open and tight states of β-actin. The open and tight states of β-actin were aligned as in Figure 4. The main chain of the phosphate-binding loops N12–C17 and D154–H161 (carbonyl groups omitted) of open and tight states of β-actin are shown in cyan and black lines, respectively. The location of the Gly15 amide group is marked. The ATP is represented by balls and sticks (cyan, open state). O1B is green and O2B is red. The divalent cation is yellow. The labelling of the oxgen atoms follows that of the tight-state PDB file 2btf. In the DNase I:α-actin structure, the labelling of the oxygen atoms is reversed. The direction of view is approximately down the crystal *b*-axis.

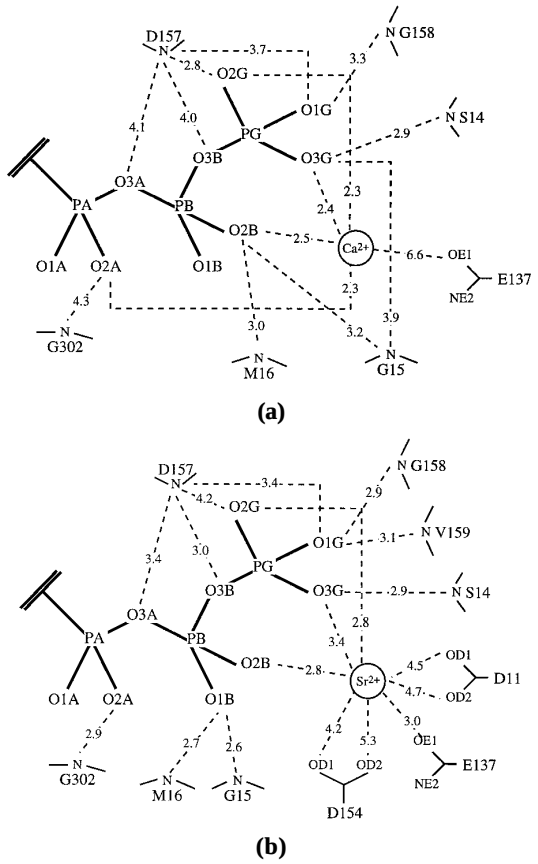

Figure 11. Distances between atoms within the ATP phosphate-binding regions for open and tight-state β-actin. Interatomic distances (Å) were determined using the program O (Jones *et al*., 1991). (a) Open state; (b) tight state.

observation that during polymerization there is a large change in the environment of the labelled residue, seen by fluorescence spectroscopy, imply that the C terminus can undergo significant changes in conformation (Frieden *et al*., 1980; Frieden & Patane, 1985; Crosbie *et al*., 1994). Changing C374 in β-actin to serine by site-directed mutagenesis affects the ability of actin to polymerize and to translocate in *in vitro* motility assays (Aspentröm *et al*., 1993). Genetic studies in yeast demonstrated that deletion of one, two or three residues from the C terminus of actin causes disturbance of increasing seriousness for the yeast phenotype (Johannes & Gallwitz, 1991). Furthermore, removal of the C-terminal residues has pronounced effects on the ATPase activity accompanying polymerization and on the structure of the actin filament as seen by electron microscopy (O'Donoghue *et al*., 1992; Orlova and Egelman, 1992, 1995; Mossakowska *et al*., 1993; Strzelecka-Golaszewska *et al*., 1995). This reinforces the notion of a physiologically important and sensitive structure at the ''barbed end'' of the actin molecule. Observations on crystalline profilin:β-actin are consistent with this possibility, since during the open to tight-state transition the environment of W356 changes significantly (Figure 3).

Linked conformational changes

Proteolytic susceptibility of the DNase I-binding loop, as well as fluorescent probes attached to C374 or to the DNase I-binding loop have been widely used to study conformational changes in actin monomers and filaments (Strzelecka-Golaszewska *et al*., 1993, Crosbie *et al*., 1995; Kim *et al*., 1995). These studies reveal a linkage between the DNase I-binding loop, the nucleotide binding cleft situated between the two major domains of actin, and the penultimate C374 of actin. As these three structural elements are spatially distant from each other in the actin monomer, it has been suggested that subdomain movements are involved in the transmittal of conformational signals from one part of the actin molecule to the other (Crosbie *et al*., 1995). This linkage phenomenon is evident also in the open to tight-state transition. Moreover, the N terminus, subdomain 2, the loops at the top of subdomain 4, and residues in the vicinity of the penultimate C-terminal cysteine residue, from different monomers are all found sandwiched in a common conformationally sensitive region of the β-actin ribbon (Figure 6). Future modelling of F-actin will be based on the premise that the active surfaces on monomers N – 1 and N + 1 (Figure 6) can be brought into contact by a combination of motions about the observed hinge-points (Figure 4(b)) within β-actin (Schutt *et al*., 1995b), accommodated by the twisting and tilting of subdomain 2 situated at the three-body site of interaction.

Profilin:β-actin in solution can be dissociated by lowering the pH. When crystals of the profilin:β-actin complex in ammonium sulphate are subjected to a drop in pH, a semicrystalline fibre pattern is observed (Schutt *et al*., 1989). This suggests that at least partial dissociation of profilin can occur in the crystals. The large intensity changes in the diffraction pattern associated with this transition must arise from even more extensive subdomain motions than those described here. Apparently, protonation of profilin H119 affects the conformationally sensitive regions found near the C termini of actin molecules organized into ribbons (see Figures 3 and 6), triggering the transition to a fibre-like state in the crystals.

It is remarkable that the application of osmotic pressure, amounting to only 60 cal / mol unit cell at 20°C, can change the unit cell dimensions as extensively as that seen in the open to collapsed-state transition. Apparently, this high degree of cooperative deformability in the crystalline state is possible because of the extensive pattern of intermolecular bonds, including the ribbon contacts and those between profilin molecules that provide ''support-columns'' for the ribbons. As a consequence, all the molecules in the crystal can respond in concert to changes in chemical or mechanical environments, as evidenced by the maintenance of sharp diffraction spots to high resolution throughout the open to tight-state transition. It is significant

that the forces applied to actin crystals by changes in osmotic pressure, in the range of 1.7×10^5 to 3.3×10^5 dynes per cm^2, are of a magnitude comparable with those known to reduce the effective diameter of actin filaments in bundles (Grazi *et al*., 1993; Schwienbacher *et al*., 1995). The apparently slight energy difference at room temperature between the open and tight states of actin is consistent with conclusions reached on the basis of detailed comparisons between open and closed states of a large number of crystalline structures. Interlocking water-mediated networks of salt-bridges, hydrogen bonds, and packing interactions between domains have been shown to be important in determining the stability and specificity of closed states (Gerstein *et al*., 1994). This suggests that the specific effect of ammonium ions (Table 1) might be to modify such interactions in the actin nucleotide-binding cleft, triggering the linked set of transitions observed in the crystals (Figure 6).

The equilibrium motion observed during the open to tight-state transition in profilin:β-actin crystals is large compared with those predicted by normal mode analysis (Tirion *et al*., 1995). Furthermore, the ability to measure the mechanical work done in collapsing the crystals into the tight state, through the application of osmotic stresses (in a range known to affect the structure of F-actin), yields the energies of the crystalline transitions, an otherwise difficult quantity to measure or to calculate for solvated protein molecules.

Functional implications of crystalline transitions

A model for the profilin-assisted assembly of actin filaments is based on the premise of coordinated subdomain movements about multiple hinge-points in β-actin ribbons (Cedergren-Zeppezauer *et al*., 1994; Schutt *et al*., 1995b). The picture suggested by the present crystallographic results is that the profilin-bound open state of β-actin, with its more solvent-exposed nucleotide, is the structural precursor presented to the barbed end of growing filaments (Pantaloni & Carlier, 1993). As the profilin:β-actin heterodimer is incorporated into the growing filament with its ribbon-like barbed end (Cedergren-Zeppezauer *et al*., 1994; Schutt *et al*., 1995b), the nucleotide becomes more deeply buried in the cleft between the two domains as in the tight state. Thus the binding energy of the nucleotide would contribute to an ordering of residues in the active site that are to participate in nucleotide hydrolysis. Subsequent release of inorganic phosphate into solution, coupled with dislodgement of profilin, would result in further rearrangements of the subdomains about the observed hinge-points, leading to a helically symmetric filament (Schutt *et al*., 1995b).

Materials and Methods

Purification of profilin:β-actin complex

Purification and crystallization of the bovine profilin:β-actin complex from calf thymus has been described (Rozycki *et al*., 1991). Thymuses from freshly killed calves (newborn to three months old) were immediately frozen on solid CO_2 for overnight shipment and stored at –80°C (Pel-Freez Biological, Rodgers, AK). In brief, the still-frozen thymus tissue was homogenized and the crude extract was clarified by ultracentrifugation. The extract was loaded onto a poly-L-proline-Sepharose column, which selectively bound the profilin and profilin:actin complex. The poly-L-proline column was eluted using 30% (v/v) dimethyl sulphoxide. The eluted protein was diluted three times with 5 mM potassium phosphate buffer (pH 7.5) and loaded onto a hydroxylapatite column (Hypatite C, even lot numbers, Clarkson Chromatography Products Inc., South Williamsport, PA), which in turn was eluted with a glycine/potassium phosphate gradient to separate profilin:β-actin from the profilin:γ-actin isoform. The eluted fractions were precipitated by dialysis against saturated ammonium sulphate and stored at 4°C. The gel-filtration step described earlier was not used here.

Crystallization of profilin:β-actin

To crystallize the profilin:β-actin complex (Rozycki *et al*., 1991), the precipitated protein was dissolved in KPO_4 buffer (5 mM potassium phosphate (pH 7.3), with 2 mM $CaCl_2$, 1 mM ATP (sodium salt) and 5 mM DTT). After clarifying the solution by centrifugation at 30,000 ***g*** for 15 minutes at 4°C, the supernatant had a concentration of approximately 10 mg/ml as determined spectrophotometrically (1 mg of profilin:β-actin/ml has an A_{290}–A_{310} of 0.63). The protein solution (1 to 1.5 ml) was dialysed in SpectraPor 7 dialysis tubing (cut-off 8000 Da, diam. 23 mm, Spectrum, Houston, TX) against 1.3 M KPO_4 buffer (pH 7.3), with 2 mM $CaCl_2$, 1 mM ATP and 5 mM DDT for six hours. This leads to polymerization of a fraction of the actin from the profilin:β-actin complex and the formation of paracrystals. After dialysis, the paracrystals were removed by centrifugation (30,000 ***g***) for 15 minutes at 4°C. The supernatant (18 to 20 mg/ml) was further clarified by centrifugation at 360,000 ***g*** for ten minutes at 4°C. If left undisturbed, microcrystals (0.1 mm, largest dimension) appeared in a few hours. Such microcrystals were used for seeding. To prevent their formation, the solution was filtered twice through a Millipore filter (0.2 μm GV disposable filter unit, diam. 13 mm, Millipore, Bedford, MA). The filtered solution often remained free of crystal formation. The final volume of concentrated, filtered protein solution was 300 to 400 μ1. A controlled amount of microseed crystals was introduced, which led to the formation of diffraction quality crystals (0.5 mm × 0.3 mm × 0.15 mm) within two to three days.

Crystals were obtained using the hanging-drop method (McPherson, 1989). The unseeded protein solution (40 μ1) was pipetted onto silanized coverslips, which then were sealed over Linbro plate wells containing dialysis buffer, and incubated at 4°C for approximately 12 hours for further equilibration. Then the coverslips with the drops of protein solution were removed from the wells and seeded by carefully pipetting about 4 μl of diluted seed solution (diluted 1:10,000 (v/v) with dialysis buffer) into the drop. Once

an optimal dilution had been found for a particular seeding solution, seeding was reproducible using that dilution. The coverslips with the seeded drops were then resealed over the Linbro plate wells containing dialysis buffer at 4°C. Diffraction quality crystals appeared in 24 hours. This technique gave the best crystals for collecting data and was used for most of the experiments.

Crystals were harvested at 4°C by gently removing them from the droplets into 3 ml of 1.5 M potassium phosphate (pH 7.3), with 1 mM ATP and 5 mM DTT in a glass vial. The concentration of potassium phosphate was raised from 1.5 M to 1.8 M by removing 2 ml of solution (after the crystals settled) and replacing it with 2 ml of 1.8 M potassium phosphate (pH 7.3), 1 mM ATP, 5 mM DTT. This was repeated three times. It was important that the pH of the 1.5 M and 1.8 M potassium phosphate solution be closely matched (± 0.02). The transfers were more successful if all the solutions and vials were equilibrated on an ice-water bath. Some crystals cracked during the transfer process, but often the fragments were large enough to be used for crystallography. After the concentration of potassium phosphate was increased, the vials were warmed slowly to room temperature by placing them in a styrofoam box with an ice-water mixture and placing the box at room temperature. After warming to room temperature, the crystals were transferred to the final open-state buffer consisting of 1.8 M KPO_4 (pH 7.50), 1 mM ATP and 5 mM DTT. Harvesting and final buffers contained no greater than 1 μM Ca^{2+}, enough to keep the divalent cation high-affinity site (K_d of 2 to 3 nM; Estes *et al*., 1992) of actin saturated, but without occupying the low-affinity sites. The crystals were stable for at least two months.

Data collection

Diffraction data were collected at the Brookhaven NSLS on the X12C beamline. The beamline was equipped with a MAR(tm) 300 mm diameter image-plate detector using a kappa goniometer under control of MARMAD (Skinner *et al*., 1993). X-ray irradiation was monochromated to 1.1 Å in both cases. All data were collected at 15°C. Integration and scaling were carried out using DENZO and SCALEPACK in the HKL suite of programs (unpublished). The 2.65 Å data set required six crystals. The overall completeness was 87.3% with an R_{merge} of 8.2% between 50.0 and 2.65 Å. Scaling statistics for the open-state crystals from SCALEPACK are summarized in Table 4. The $P2_12_12_1$ unit cell for the open-state crystals had dimensions of 38.14 Å × 72.45 Å × 185.7 Å. Scaled intensity data were converted to F_{obs} using TRUNCATE (French & Wilson, 1978). The overall *B*-factor of the data set was 48.3 Å^2.

Table 4. Summary of scaling statistics for merging the data set for the open state of profilin:β-actin crystals

Range (Å)	$\langle I \rangle$	σ (*I*)	No. obs.	%obs.	R_{merge}
50.00–7.19	9515.8	465.2	811	88.7	0.049
7.19–5.71	3911.7	186.4	790	93.7	0.059
4.99–4.53	4512.9	209.5	767	94.6	0.067
4.53–4.21	6351.7	280.8	764	95.7	0.069
4.21–3.96	4803.8	238.7	755	93.7	0.075
3.96–3.76	3754.1	218.4	732	94.6	0.087
3.76–3.60	3101.6	207.3	763	94.4	0.090
3.60–3.46	2539.9	199.1	717	94.1	0.102
3.46–3.34	2169.2	200.6	742	92.8	0.106
3.34–3.23	1807.4	199.4	714	91.1	0.114
3.23–3.14	1309.6	198.3	681	87.4	0.138
3.14–3.06	1264.2	199.6	697	88.5	0.137
3.06–2.98	939.2	188.2	662	84.8	0.159
2.98–2.92	901.7	197.1	618	81.7	0.171
2.92–2.85	809.5	204.2	609	76.5	0.179
2.85–2.80	705.1	188.8	595	77.2	0.215
2.80–2.74	601.4	191.7	575	76.2	0.224
2.74–2.70	582.8	211.4	588	74.6	0.216
2.70–2.65	470.4	198.9	533	69.0	0.267
All data	3048.8	225.9	13,869	87.3	0.082

The results are broken down into resolution bins showing average intensity, $\langle I \rangle$, standard deviation in *I*, σ (*I*), number of observations, percentage reflections observed over expected and $R_{merge} = \Sigma_i |I_i - \langle I_i \rangle| / \Sigma_i I_i$ where I_i is intensity of reflection *i* and $\langle I_i \rangle$ average intensity of *i*.

Structure determination

Atomic coordinates of tight-state profilin:β-actin (Schutt *et al*., 1993; PDB entry pdb2btf.ent) were used as a search model for molecular replacement as implemented in XPLOR (Brünger, 1993) using data in the range 8.0 to 4.0 Å with a 2σ cut-off (i.e. $F_{obs} > 2\sigma(F_{obs})$). The rotation search gave a maximum for the rotation function of 3.2502 for a rotation of (0 0 0). The top 6000 solutions to the rotation functions (after clustering) were subjected to Patterson Correlation (PC) Refinement (Brünger, 1990). The maximum peak was observed with the (0 0 0) rotation, which refined to Eulerian angles $\alpha = 40.4°$, $\beta = 0.5°$, $\gamma = 319°$ and a PC value of 0.143. This solution to the rotation function was used in the translation search resulting in a maximum of the translation function of 0.400, which was 12σ above the mean of 0.134. After a final rigid body refinement (using data in the 8 to 4 Å range), the *R*-factor was 0.4558.

A $2F_o - F_c$ map of the open-state crystals, calculated with data from 8 to 3.1 Å using phases obtained by molecular replacement, showed poor density for residues 1 to 7, 22 to 102 and 194 to 203 of actin. The molecular replacement solution structure excluding these regions was again subjected to rigid body refinement using data in the 8.0 to 4.0 Å range, yielding an *R*-factor of 0.4578. The majority of the residues in the excluded regions of the molecule were rebuilt using the modelling program O (Jones *et al*., 1991) into a $2F_o - F_c$ map with phases obtained from the partial structure using data in the range 8.0 to 3.1 Å. With the newly added residues, another $2F_o - F_c$ electron density map was calculated, and most of the excluded residues were placed in reasonable electron density with the exception of residues 2 to 3, 42 to 48 and 199 to 203. The partial structure of the open-state crystals was subjected to 40 cycles of conjugate gradient minimization in XPLOR using data between 8.0 and 3.1 Å. The data set was modified by the exclusion of 10% of the data to enable R_{free} calculations. The initial R_{free} and *R* for the partial structure were 0.4574 and 0.4442, respectively. After 40 cycles, $R_{free} = 0.4489$ and $R = 0.3954$ in the range 8.0 to 3.1 Å. A new $2F_o - F_c$ map was generated using the refined partial structure for phase calculation. The remaining residues were added at this point. The completed structure of the open-state crystals was subjected to simulated annealing refinement with data in the range 8.0 to 2.8 Å using the slow-cooling protocol starting at 3000 K (Brünger, 1993). After a restrained *B*-factor refinement, R_{free} for the open-state was 0.3952 and *R* was 0.2417.

The open-state structure was rebuilt into omit maps after phase refinement by simulated annealing (SA) using data in the range 8.0 to 2.8 Å (Hodel *et al*., 1992). The

Table 5. The *R*-factors of the final open-state of the profilin:β-actin structure ($F > 2\sigma$)

Range (Å)	No. obs.	*R*	R_{cum}
8.00–4.91	1642	0.2100	0.2100
4.91–4.06	1607	0.1485	0.1767
4.06–3.60	1576	0.1694	0.1746
3.60–3.30	1514	0.2022	0.1796
3.30–3.08	1450	0.2197	0.1844
3.08–2.91	1319	0.2554	0.1902
2.91–2.77	1231	0.2747	0.1955
2.77–2.65	1165	0.3153	0.2013

SA-omit maps were calculated using excluded spheres of 9 Å covering, in succession, profilin, actin subdomain 3, and subdomain 1 excluding residues 2 to 7, 22 to 32 and 71 to 102. The remainder of the structure was built back into the $2F_o - F_c$ map based on the partial structure as described above. Simulated annealing refinement of the rebuilt structure to 2.8 Å resolution using the 3000 K protocol yielded an unacceptably high value for R_{free} of 0.40. After eliminating the DNase I binding loop of actin (residues 39 to 51), and the three N-terminal residues 2 to 4, a simulated annealing refinement yielded a partial structure with R_{free} of 0.3457 and *R* of 0.1908 after restrained *B*-factor refinement of individual atoms. The missing regions were built back into the $2F_o - F_c$ map based on the refined partial structure using data from 8.0–3.8 Å. The completed molecular model was subjected to a 1000 K simulated annealing refinement using data to a resolution limit of 2.65 Å, yielding an R_{free} of 0.3412 and an *R* of 0.1983. The β-actin part of the open-state complex was then rebuilt into omit maps calculated with structure factors refined by simulated annealing. Each successive electron density map was calculated with 20 consecutive residues omitted. After rebuilding, the entire β-actin molecule was conjugate-gradient minimized with restrained *B*-factor refinement to an R_{free} of 0.3295 and an *R* of 0.2040. Before a final cycle of refinement, the calcium ion was placed into density near the ATP phosphate groups. The open-state profilin:β-actin structure with Ca^{2+} was subjected to conjugate-gradient refinement (*B*-factors included) to give a final R_{free} of 0.3278 and an *R* of 0.2013. Table 5 shows the *R*-factor as a function of resolution. The estimated error in coordinates is approximately 0.3 Å, as shown in a Luzzati plot (Luzzati, 1952; Chik, 1996). Figure 12 shows the main-chain *B*-factor as a function of residue number. The average main-chain temperature factor for β-actin was 29.8 $Å^2$. Profilin has an average main-chain temperature factor of 17.4 $Å^2$. The final open-state profilin:β-actin structure has an average rms bond length and bond angle deviation of 0.015 Å and 2.11°, respectively, from ideality, as calculated in XPLOR.

Chemical dependence of the unit cell

To study the effect of varying pH, potassium phosphate concentration, and cations (Na^+, K^+ and NH_4^+) crystals were transferred directly from the open state into the desired final state. In the osmotic pressure experiments, however, it was found that one intermediate step was necessary. After transferring the crystals into new solution conditions, they were allowed to equilibrate for at least 18 hours before either next transfer or X-ray diffraction analysis was performed.

The variation of the unit cell dimensions of profilin:β-actin crystals with pH was studied by transferring crystals from their initial open-state buffer (1.8 M KPO_4 (pH 7.3), 1 mM ATP, 5 mM DTT) directly into a new open-state buffer with the pH of interest. The test buffers were made by mixing 1.8 M K_2HPO_4 with a 1.8 M KPO_4 buffer at pH 6.0 (86.0 g of KH_2PO_4 and 46.7 g of K_2HPO_4 to 500 ml). By varying the proportions of the two solutions a range of buffers with varying pH values was made. The pH was measured using a ROSS(tm) glass electrode from Orion (model 81-02). Finally, the appropriate amounts of solid ATP and DTT were added to give 1 mM ATP and 5 mM DTT. The unit cell dimensions of the crystals were determined over a range of KPO_4 concentrations (1.8 M to 3.6 M). The various buffer solutions were made by diluting a 3.6 M KPO_4 solution (27.2 g of KH_2PO_4 and 117.6 g of K_2HPO_4 to 500 ml) and adding the appropriate amounts of ATP and DTT. The effects of different cations were studied in open-state buffers with the addition of 2.0 M NaCl, 1.5 M KCl or 2.0 M NH_4Cl. For NaCl and KCl modified open-state buffers, the pH was adjusted to 7.3 with concentrated HCl. The NH_4Cl was left at pH 7.0.

By varying the osmotic pressure, it was possible to estimate the work needed to change the cell dimensions. This technique relies on the partitioning of a hydrophilic stressing agent from the system of interest (Parsegian *et al*., 1986). The osmotic stressing agents, for example polyethylene glycol (PEG) and dextran, act to dehydrate the sample. The osmotic pressure times the change in water volume of the system gives the work done on the system. Polyethylene glycol and dextran were both insoluble in the open-state potassium phosphate buffer. However, 60 kDa dextran (Fluka Chemie AG, Switzerland) could be dissolved in 1.75 M $(NH_4)_2SO_4$, 10 mM bis-Tris base, 1 mM ATP and 5 mM DTT (final pH 7.1) to a concentration of 7.5 g/100 ml. Therefore, open-state crystals were first transferred into ammonium sulphate-containing buffers. This transfer resulted in a slight shrinking of the unit cell. After equilibrating the crystals with this solution for 18 hours, they were directly transferred into ammonium sulphate-containing buffer solutions containing different concentrations of 60 kDa dextran. The range of dextran concentrations studied was from 0 g/100 ml to 7.5 g/100 ml (approx. 0% to 7%, w/w). Transferring crystals into dextran concentrations higher than 3 g/100 ml resulted in extensive cracking, but determination of unit cell dimensions could be made using fragments of the crystals.

X-ray data for the unit cell variation studies were collected using a GX-21 (Enraf-Nonius, Bohemia, NY) generator with a rotating Cu anode. The cathode was fitted with a 0.3 mm × 3 mm focal cup and the accelerating voltage was 40 kV with a filament current of 95 mA. The CuKα radiation was monochromated using a graphite crystal. Diffracted radiation was collected using a FAST (Enraf-Nonius, Bohemia, NY) electronic area-detector. The detector was set at THETA = 0 and DIST ≈ 100 mm. Unit cell determinations consisted of collecting two 5° sweeps of data taken 90° apart. A single data frame consisted of a 0.1° sweep with an exposure time of 60 to 90 seconds. The data were collected and analysed using MADNES (Messerschmidt and Pflugrath, 1987). Spots with an $I/\sigma I > 5$ were located using the FIND level of MADNES. The collected spots were refined in the REFINE level to obtain the unit cell parameters. A single crystal typically gave over 150 reflections for use in REFINE. Accepted REFINE results (less than 2% reflections rejected) were those that had a rmsDEG < 0.05 (typically < 0.03). The reported error in cell dimensions was the standard deviation reported by MADNES in the

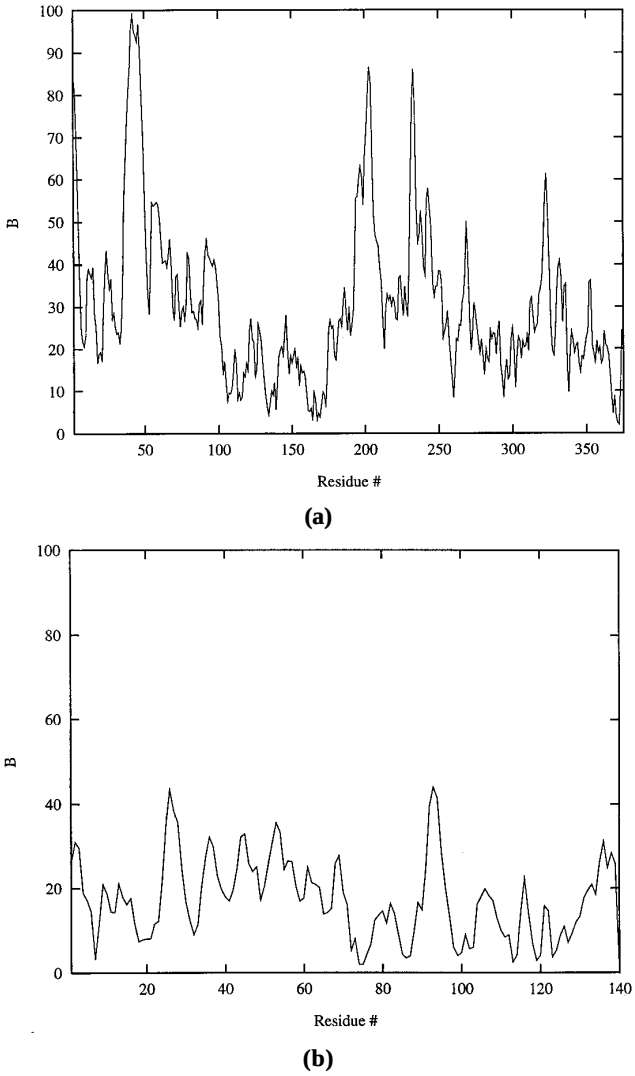

Figure 12. Main-chain *B*-factors (Å^2) for (a) open-state β-actin and (b) for profilin.

final refinement cycle, fixing all parameters except cell dimensions and crystal misset angles.

Acknowledgements

We acknowledge the insight and assistance of Dr Nalin Goonesekere, Dr Jim Myslik, Dr Michael Rozycki, Dr Robert M. Sweet and Dr Nancy Vogelaar. This work was supported by grants to C.E.S. from the National Institutes of Health (U.S.A.) and to U.L. from the Swedish Cancer Foundation, the Swedish Natural Science Research Council and The Fulbright Commission.

References

Aspenström, P., Schutt, C. E., Lindberg, U. & Karlsson, R. (1993). Mutations in β-actin: influence on polymer formation and on interactions with myosin and profilin. *FEBS Letters*, **329**, 163–170.

AL-Khayat, H. A., Yagi, N. & Squire, J. M. (1995). Structural changes in actin-tropomyosin during muscle regulation: computer modelling of low-angle X-ray diffraction data. *J. Mol. Biol.* **252**, 611–632.

Bennett, W. S., Jr & Steitz, T. A. (1980). Structure of a complex between yeast hexokinase A and glucose. II. Detailed comparisons of conformation and active site configuration with the native hexokinase B monomer and dimer. *J. Mol. Biol.* **140**, 211–230.

Berridge, M. J. (1993). Inositol trisphosphate and calcium signalling. *Nature*, **361**, 315–325.

Brünger, A. T. (1990). Extension of molecular replacement: a new search strategy based on patterson correlation refinement. *Acta Crystallog. sect. A*, **46**, 46–57.

Brünger, A. T. (1993). *XPLOR Version 3.1 Manual*, Yale University, New Haven, CT.

Carlsson, L. (1979). Cell motility: the possible role of unpolymerized actin. PhD thesis, Uppsala University, ISBN 91-554-0956-3.

Carlsson, L., Nyström, L.-E., Lindberg, U., Kannan, K. K., Cid-Dresdner, H., Lövgren, S. & Jörnvall, H. (1976). Crystallization of a non-muscle actin. *J. Mol. Biol.* **105**, 353–366.

Carlsson, L., Nyström, L.-E., Sundkvist, I., Markey, F. & Lindberg, U. (1977). Actin polymerizability is influenced by profilin, a low molecular weight protein in non-muscle cells. *J. Mol. Biol.* **115**, 465–483.

Cassimeris, L., Safer, D., Nachmias, V. T. & Zigmond, S. H. (1992). Thymosin β4, sequesters the majority of G-actin in resting human polymorphonuclear leukocytes. *J. Cell Biol.* **119**, 1261–1270.

Cedergren-Zeppezauer, E. S., Goonesekere, N. C. W., Rozycki, M. D., Myslik, J. C., Dauter, Z., Lindberg, U. & Schutt, C. E. (1994). Crystallization and structure determination of bovine profilin at 2.0 Å resolution. *J. Mol. Biol.* **240**, 459–475.

Chik, J. K. (1996). Solid-state transformations of crystalline bovine profilin:β-actin complex at atomic resolution. PhD thesis, Princeton University, Princeton, NJ.

Cini, R., Burla, M. C., Nunzi, A., Polidori, G. P. & Zanazzi, P. F. (1984). Preparation and physicochemical properties of ternary complexes formed between adenosine 5'-t triphosphate acid, bis(2-pyridyl)amine and divalent metal ions. Crystal and molecular structures of the compounds containing Mg^{II} and Ca^{II}. *J. Chem. Soc. Dalton Trans*. 2467–2476.

Collaborative Computational Project, No. 4 (1994). The CCP4 suite: programs for protein crystallography. *Acta Crystallog. sect. D*, **50**, 760–763.

Crosbie, R. H., Miller, C., Cheung, P., Goodnight, T., Muhlrad, A. & Reisler, E. (1994). Structural connectivity in actin: effect of C-terminal modifications on the properties of actin. *Biophys. J.* **67**, 1957–1964.

Egelman, E. H. & Orlova, A. (1995). New insights into actin filament dynamics. *Curr. Opin. Struct. Biol.* **5**, 172–180.

Estes, J. E., Selden, L. A., Kinosian, H. J. & Gershman, L. C. (1992). Tightly-bound divalent cation of actin. *J. Muscle Res. Cell Motil.* **13**, 272–284.

Fievez, S. & Carlier, M.-F. (1993). Conformational changes in subdomain-2 of G-actin upon polymerization into F-actin and upon binding myosin subfragment-1. *FEBS Letters*, **316**, 186–190.

Flaherty, K. M., McKay, D. B., Kabsch, W. & Holmes, K. C. (1991). Similarity of the three-dimensional structures of actin and the ATPase fragment of a

70-kDa heat shock cognate protein. *Proc. Natl Acad. Sci. USA*, **88**, 5041–5045.

French, S. & Wilson, K. (1978). On the treatment of negative intensity observations. *Acta Crystallog. sect. A*, **34**, 517–525.

Frieden C. & Patane, K. (1985). Differences in G-actin containing bound ATP or ADP: the Mg^{2+}-induced conformational change requies ATP. *Biochemistry*, **24**, 4192–4196.

Frieden, C., Lieberman, D. & Gilbert, H. R. (1980). A fluorescent probe for conformational changes in skeletal muscle G-actin. *J. Biol. Chem.* **255**, 8991–8993.

Gerstein, M., Lest, A. M. & Chothia, C. (1994). Structural mechanisms for domain movements in proteins. *Biochemistry*, **33**, 6739–6749.

Grazi, E., Schwienbacher, C. & Magri, E. (1993). Osmotic stress is the main determinant of the diameter of the actin filament. *Biochem. Biophys. Res. Commun.* **197**, 1377–1381.

Goldschmidt-Clermont, P. J., Machesky, L. M., Baldassare, J. J. & Pollard, T. D. (1990). The actin-binding protein profilin binds to PtdIns(4,5)P_2 and inhibits its hydrolysis by phospholipase C. *Science*, **247**, 1575–1578.

Goldschmidt-Clermont, P. J., Kim, J. W., Machesky, L. M., Rhee, L. M. & Pollard, T. D. (1991). Regulation of phosphlipase C-γ1 by profilin and tyrosine phosphorylation. *Science*, **251**, 1231–1233.

Goldschmidt-Clermont, P. J., Furman, M. I., Wachsstock, D., Safer, D., Nachmias, V. T. & Pollard, T. D. (1992). The control of actin nucleotide exchange by thymosineβ4 and profilin. A potentially regulatory mechanism for actin polymerization in cells. *Mol. Biol. Cell*, **3**, 1015–1024.

Hartwig, J. H., Bokoch, G. M., Carpenter, C. L., Janmey, P. A., Taylor, L., Toker, A. & Stossel, T. P. (1995). Thrombin receptor ligation and activated rac uncap actin filament barbed ends through phosphoinositide synthesis in permeabilized human platelets. *Cell*, **82**, 643–653.

Hegyi, G., Premecz; G., Sain, B. & Muhlrad, A. (1974). Selective carbethoxylation of the histidine residues of actin by diethypyrocarbonate. *Eur. J. Biochem.* **44**, 7–12.

Hitchcock, S., Carlsson, L. & Lindberg, U. (1976). Depolymerization of F-actin by deoxyribonuclease I. *Cell*, **7**, 531–542.

Hodel, A., Kim, S.-H. & Brünger, A. T. (1992). Model bias in macromolecular crystal structures. *Acta Crystallog. sect. A*. **48**, 851–858.

Holmes, K. C., Popp, D., Gebhard, W. & Kabsch, W. (1990). Atomic model of the actin filament. *Nature*, **347**, 44–49.

Hutchinson, E. G. & Thornton, J. M. (1994). A revised set of potentials for β-turn formation in proteins. *Protein Sci.* **3**, 2207–2216.

Johannes, F. J. & Gallwitz, D. (1991). Site-directed mutagenesis of the yeast actin gene: a test for actin function in vivo. *EMBO J.* **10**, 3951–3958.

Jones, A. T., Zou, J.-Y., Cowan, S. W. & Kjeldgaard, M. (1991). Improved methods for building protein models in electron density maps and the location of errors in these models. *Acta Crystallog. sect. A*, **47**, 110–119.

Kabsch, W. (1976). A solution for the best rotation to relate two sets of vectors. *Acta Crystallog. sect. A*, **32**, 922–923.

Kabsch, W. & Holmes, K. E. (1995). The actin fold. *FASEB J.* **9**, 167–174.

Kabsch, W., Mannherz, H.-G., Suck, D., Pai, E. F. & Holmes, K. C. (1990). Atomic structure of the actin:DNase I complex. *Nature*, **347**, 37–44.

Kim, E., Motoki, M., Seguro, K., Muhlrad, A. & Reisler, E. (1995). Conformational changes in subdomain 2 of G-actin: fluorescence probing by dansyl ethylenediamine attached to Gln-41. *Biophys. J.* **69**, 2024–2032.

Korn, E. D., Pantaloni, D. & Carlier, M.-F. (1987). Actin polymerization and ATP hydrolysis. *Science*, **238**, 638–644.

Kraulis, P. J. (1991) MOLSCRIPT: a program to produce both detailed and schematic plots of protein structures. *J. Appl. Crystallog.* **24**, 946–950.

Lassing, I. & Lindberg, U. (1985). Specific interaction between phosphatidylinositol 4,5-bisphosphate and profilactin. *Nature*, **314**, 472–474.

Lassing, I. & Lindberg, U. (1988). Specificity of interaction between phosphatidylinositol 4,5-bisphosphate and the profilin:actin complex. *J. Cell. Biochem.* **37**, 255–267.

Lazarides, E. & Lindberg, U. (1974). Actin is the naturally occurring inhibitor of DNase I. *Proc. Natl Acad. Sci. USA*, **71**, 4742–4646.

Lindberg, U., Schutt, C. E., Hellsten, E., Tjäder, A.-C. & Hult, T. (1988). The use of poly(l-proline) in the isolation of profilin and profilactin complexes. *Biochim. Biophys. Acta*, **967**, 391–400.

Luzzati, V. (1952). Traitement statistique des erreurs dans la determinations des structures cristallines. *Acta Crystallog.* **5**, 802–810.

Machesky, L. M. & Pollard, T. D. (1993). Profilin as a potential mediator of membrane-cytoskeleton communication. *Trends Cell Biol.* **3**, 381–385.

McLaughlin, P. J., Gooch, J. T., Mannherz, H.-G. & Weeds, A. G. (1993). The atomic structure of gelsolin segment 1: actin complex and the mechanism of filament severing. *Nature*, **364**, 685–692.

McPherson. A. (1989). *Preparation and Analysis of Protein Crystals*, chapt. 4, Robert E. Krieger Publishing Co., Malabar, FL.

Messerschmidt, A. & Pflugrath, J. W. (1987). Crystal orientation and X-ray pattern prediction routines for area-detector diffractometer systems in macromolecular crystallography. *J. Appl. Crystallog.* **20**, 306–315.

Milligan, R. A., Whittaker, M. & Safer, D. (1990). Molecular structure of F-actin and location of surface binding sites. *Nature*, **348**, 217–221.

Mockrin, S. C. & Korn, E. D. (1980). Acanthamoeba profilin interacts with G-actin to increase the rate of exchange of actin-bound adenosine 5'-triphosphate. *Biochemistry*, **19**, 5359–5362.

Mossakowska, M., Moraczewska, J., Khaitlina, S. & Strzelecka-Golaszewska, H. (1993). Proteolytic removal of three C-terminal residues of actin alters the monomer-monomer interactions. *Biochem. J.* **289**, 897–902.

O'Donoghue, S. I., Miki, M. & dos Remedios, C. G. (1992). Removing the two C-terminal residues of actin affects the filament structure. *Arch. Biohem. Biophys.* **293**, 110–116.

Oosawa, F. (1983). Macromolecular assembly of actin. In *Muscle and Nonmuscle Motility* (Stracher, A., ed.), pp. 151–216, Academic Press, London.

Orlova, A. & Egelman, E. H. (1992). Structural basis for the destabilization of F-actin by phosphate release following ATP hydrolysis. *J. Mol. Biol.* **227**, 1043–1053.

Orlova, A. & Egelman, E. H. (1995). Structural dynamics of F-actin I. Changes in the C terminus. *J. Mol. Biol.* **245**, 582–597.

Pantaloni, D. & Carlier, M.-F. (1993). How profilin promotes actin filament assembly in the presence of thymosine β4. *Cell*, **75**, 1007–1014.

Parsegian, V. A., Rand, R. P., Fuller, N. L. & Rau, D. C. (1986). Osmotic stress for the direct measurement of intermolecular force. *Methods Enzymol.* **127**, 400–416.

Pring, M., Weber, A. & Bubb, M. R. (1992). Profilin-actin complexes directly elongate actin filaments at the barbed end. *Biochemistry*, **31**, 1827–1836.

Reichstein, E. & Korn, E. D. (1979). *Acanthamoeba* profilin. *J. Biol. Chem.* **254**, 6174–6179.

Rossmann, M. G. & Blow, D. M. (1958). The detection of sub-units within the crystallographic asymmetric unit. *Acta Crystallog.* **15**, 24–31.

Rozycki, M. D., Schutt, C. E. & Lindberg, U. (1991). Affinity chromatography-based purification of profilin:actin. *Methods Enzymol.* **196**, 100–118.

Rozycki, M. D., Myslik, J. C., Schutt, C. E. & Lindberg, U. (1994). Structural aspects of actin-binding proteins. *Curr. Opin. Cell Biol.* **6**, 87–95.

Safer, D., Elzinga, M. & Weber, A. (1991). Thymosin β4, and Fs, an actin-sequestering peptide, are indistinguishable. *J. Biol. Chem.* **266**, 4029–4032.

Schutt, C. E., Lindberg, U., Myslik, J. & Strauss, N. (1989). Molecular packing in profilin-actin crystals and its implications. *J. Mol. Biol.* **209**, 735–746.

Schutt, C. E., Myslik, J. C., Rozycki, M. D., Goonesekere, N. C., W. & Lindberg, U. (1993). The structure of crystalline profilin:β-actin. *Nature*, **365**, 810–816.

Schutt, C. E., Rozycki, M. D., Chik, J. & Lindberg, U. (1995a). Structural studies on the ribbon-to-helix transition in profilin:actin crystals. *Biophys. J.* **68**, 12s–18s.

Schutt, C. E., Rozycki, M. D., Myslik, J. C. & Lindberg, U. (1995b). A discourse on modelling F-actin. *J. Struct. Biol.* **115**, 186–198.

Schwienbacher, C., Magri, E., Trombetta, G. & Gratzi, E. (1995). Osmotic properties of the calcium-regulated actin filament. *Biochemistry*, **34**, 1090–1095.

Schwyter, D. H., Kron, S. J., Toyoshima, Y. Y., Spudich, J. A. & Reisler, E. (1990). Subtilisin cleavage of actin inhibits in vitro sliding movement of actin filaments over myosin. *J. Cell Biol.* **111**, 465–470.

Segura, M. & Lindberg, U. (1984) Separation of non-muscle isoactins in the free form or as profilactin complexes. *J. Biol. Chem.* **259**, 3949–3954.

Skinner, J. M., Pflugrath, J. W. & Sweet, R. M. (1993). Development of a GUI for an existing command-line driven program. *Proc. of SHARE 80 Winter Meeting 1993*, **1**, 210.

Strzelecka-Golaszewska, H., Moraczewska, J., Khaitlina, S. Y. & Mossakowska, M. (1993). Localization of the tightly bound divalent-cation-dependent and nucleotide-dependent conformation changes in G-actin using limited proteolytic digestion. *Eur. J. Biochem.* **211**, 731–742.

Strzelecka-Golaszewska, H., Mossakowska, M., Wo'zniak, A., Moraczewska, J. & Nakayama, H. (1995). Long-range conformational effects of proteolytic removal of the last three residues of actin. *Biochem. J.* **307**, 527–534.

Tardif, M., Huang, S., Redmond, T., Safer, D., Pring, M. & Zigmond, S. (1995). Actin polymerization induced by GTPγS in permeabilized neutrophils is induced and maintained by free barbed ends. *J. Biol. Chem.* **270**, 28075–28083.

Tirion, M. M., ben-Avraham, D., Lorenz, M. & Holmes, K. C. (1995). Normal modes as refinement parameters for the F-actin model. *Biophys. J.* **68**, 5–12.

Edited by I. A. Wilson

(Received 3 May 1996; received in revised form 23 July 1996; accepted 26 July 1996)